Journal of Fluorescence
https://doi.org/10.1007/s10895-023-03454-2

RESEARCH

Sensitive Detections of Sodium Dichloroisocyanurate and Rosmarinic Acid by Polyvinylpyrrolidone Coated Copper Nanoclusters

Jianhua Kuang[1] · Qingqing Hu[1] · Yao Feng[1] · Jingxue Yuan[1] · Zhengjun Cheng[1,2]

Received: 23 August 2023 / Accepted: 26 September 2023

Abstract

In this article, the water-soluble blue-light-emitting copper nanoclusters (CuNCs) were prepared by polyvinylpyrrolidone (PVP) and ascorbic acid as templating and reducing agents, respectively. The optimization of synthesis conditions of PVP-CuNCs were studied and analyzed. And the quantum yield of the PVP-CuNCs was calculated to be 14.97%. It had good specificity and exceptionally sensitive detection for sodium dichloroisocyanurate (DCCNa)/rosmarinic acid (RA), with a linear response range of 0.030–2.400/0.030–0.900 μM and corresponding LOD value of 10.766/8.985 nM. Moreover, the fluorescent reaction mechanisms of the PVP-CuNCs-DCCNa and PVP-CuNCs-DCCNa-RA systems were discussed, and the sensing probe could be effectively used for the assays of DCCNa and RA in genuine samples, whose results were acceptable.

Keywords Copper nanoclusters · Sodium dichloroisocyanurate · Rosmarinic acid · Mechanism

Introduction

Sodium dichloroisocyanurate (DCCNa), as 1-sodium-3,5-dichloro-1,3,5-triazine-2,4,6-trione, is widely used in the treatment of industrial circulating water, the cleaning and sterilization of the food, and disinfection of the agricultural industry because of its oxidative properties [1, 2]. As a germicidal and sterilizing agent, it has strong disinfection capabilities, a wide range of applications, and low toxicity [3]. Although the toxicity of DCCNa is relatively small, excessive inhalation contact has toxic effect on the human body's lungs [4], and it will produce a large amount of water-insoluble reaction residues cyanuric acid, which may cause secondary harm in the process of disinfection. For example, cyanuric acid can cause kidney damage, disrupt amino acid metabolism, and so on [5]. Furthermore, it has been listed as a drinking water pollutant candidate by the United States Environmental Protection Agency [6]. As a result, the safety performance of DCCNa cannot be ignored, and it's important to establish a quick and easy method to monitor DCCNa.

Rosmarinic acid (RA) is an organic compound widely present in plants, and it belongs to phenolic compounds, which is synthesized by caffeic acid and 3,4-dihydroxyphenyl lactic acid [7]. RA has a wide range of applications in food, medicine, cosmetics, and other fields. For example, in the realm of the food industry, RA is frequently employed as a natural antioxidant [8]. In the realm of pharmaceutical research, RA has garnered considerable interest due to its array of biological activities, including antioxidative, anti-inflammatory, antibacterial, anticoagulant and antitumor properties [9–11]. Similarly, due to its possession of these characteristics, it can be utilized in the production of skin-care cosmetics [12]. In short, RA has many benefits and potential applications that deserve further study by researchers. In an effort to better understand and utilize it efficiently, it is significantly important to establish a simple and sensitive RA detection platform.

So far, there are fewer detection methods for DCCNa, and it is mainly the determination of cyanuric acid as well as hypochlorous acid of its decomposition products. For example, liquid chromatography-mass spectrometry (LC-MS) and gas chromatography-mass spectrometry (GS-MS) were used for the detection of cyanuric acid [13, 14]. And flow injection analysis (FIA) and chemiluminescence analysis were used for the detection of hypochlorous acid [15, 16]. But

✉ Zhengjun Cheng
ncczj1112@126.com

[1] Chemical Synthesis and Pollution Control Key Laboratory of Sichuan Province, China West Normal University, Nanchong 637002, China

[2] Institute of Applied Chemistry, China West Normal University, Nanchong 637002, China

Published online: 26 October 2023

there are many techniques for detecting RA concentrations, such as high-performance liquid chromatography (HPLC) [17], high-performance thin-layer chromatography (HPTLC) [18], differential pulse voltammetry (DPV) [19], ultraviolet-visible spectroscopy [12], and so on. However, these methods may have some problems, such as requiring complex sample preparation, specialized operators to operate instruments, time-consuming, or low sensitivity. Compared with these methods, the fluorescence method is relatively simple and highly sensitive [20]. Therefore, it is necessary to establish a new and simple method to detect the concentrations of DCCNa and RA.

Over the past few decades, various research teams have developed different materials as fluorescence sensors, such as organic dyes [21], semiconductor quantum dots (QDs) [22–24], and metal nanoclusters (MNCs) [25]. Among them, MNCs are a class of new nanomaterials, consisting of several to several hundred metal atoms, and their particle sizes are usually less than 3 nm [25]. This new type of fluorescent nanomaterial due to its small size, low toxicity, good biocompatibility, and excellent optical performance features was widely used in the fields of chemical sensing [26], bioimaging [27], catalysis [28], and other fields. Copper is rich and inexpensive compared to precious metals (Au/Ag), so CuNCs are attracted much attention. Up until now, many ways were employed to synthesize CuNCs. For example, Kang et al. [29] used N-acetyl-L-cysteine (NAC) as a reducing agent and stabilizer to effectively synthesize CuNCs through the sonochemical method, and it could detect Ag^+. Yu et al. [30] synthesized OVA-CuNCs using egg albumin ovalbumin (OVA) and 2-mercaptobenzimidazole as raw materials through one-pot method and it was used to detect RA sensitively. Zou et al. [20] synthesized Trp-CuNCs using D-tryptophan as a ligand through a rapid microwave-assisted method, and it was used for the detection of tetracycline. It's well known that the polymers contain a large number of functional groups, which can be complexed with metals. Up to now, CuNCs were prepared by PVP as a ligand, but it has not been used for the detection of DCCNa/RA.

Hence, PVP-coated copper nanoclusters (PVP-CuNCs) were prepared by one-step method (Fig. 1), and the synthesis and detection conditions were optimized. Based on the quenching effect of DCCNa on PVP-CuNCs, an efficient method for detecting DCCNa/RA was established and used in real products.

Experimental Sections

Materials and Instruments

Fourier transform infrared (FTIR) spectra were recorded by Nicolet-6700 FT-IR spectrometer (Thermo Fisher Scientific, USA) based on potassium bromide sheets and were measured in the range of 400–4000 cm^{-1}. The remaining materials and instruments were placed in the Supporting Information section.

Synthesis of PVP-CuNCs

The PVP-CuNCs were prepared by slightly modified previous literature reports [31]. In short, in the first place, 0.2 g of PVP (Mr = 58000) and 8.0 mL of ultrapure water were mixed fully at

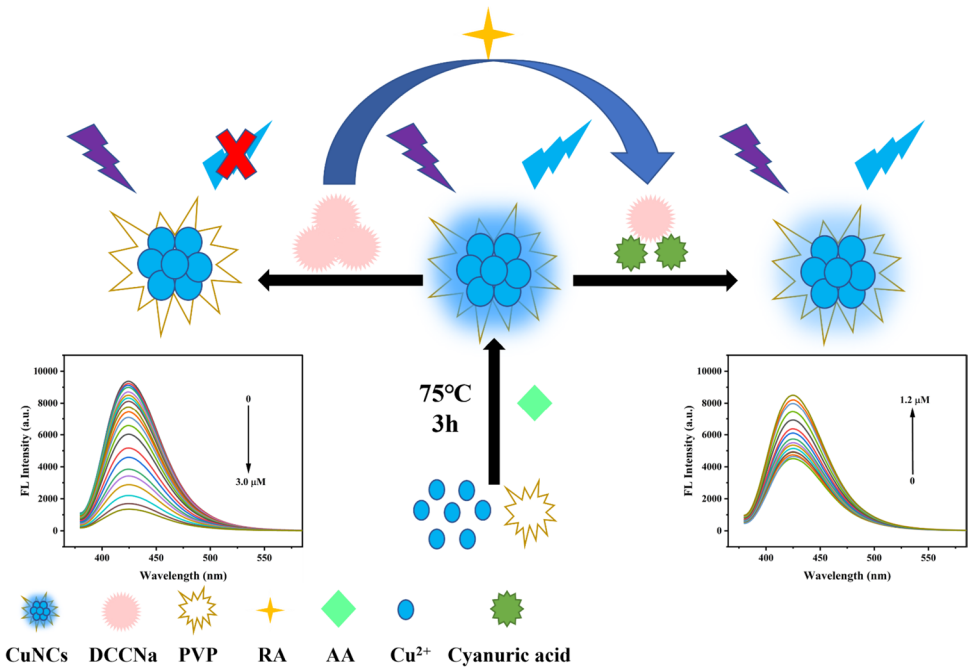

Fig. 1 The illustration of the synthesis of PVP-CuNCs and detection of DCCNa/RA by PVP-CuNCs

25℃, and then $CuSO_4 \cdot 5H_2O$ (1.0 mL, 10 mM) and AA (1.0 mL, 100 mM) were added into the mixture. Later, pH of the above mixture was adjusted to 3.5 by HCl or NaOH (1.0 M) and stirred for 3 hours at 75 ℃. After that, the solution was cooled to room temperature and purified for 24 hours with a dialysis membrane (MWCO of 8000 Da). Finally, it was stored in a refrigerator at 4 ℃ for subsequent experiments.

Quantum Yield Calculation

The calculation method of the quantum yield was displayed in the Supporting Information.

Fluorescence Detection Process of DCCNa and RA

For determining DCCNa, a series of DCCNa solutions (0.06 mM) in different volumes (0, 1.5, 3.0, 6.0, 9.0, 12.0, 15.0, 20.0, 25.0, 30.0, 35.0, 45.0, 55.0, 65.0, 75.0, 85.0, 95.0, 105.0, 120.0, 135.0 and 150.0 μL) were added to 50 μL of PVP-CuNCs solution in 10 mL plastic centrifuge tubes. Then the BR buffer solution (pH = 4) was added to set the volume to 3 mL. Afterward, the mixture was fully reacted at room temperature for 1.0 min, and corresponding fluorescence spectra were recorded at an excitation wavelength of 345 nm, whose excitation/emission slit was kept at 5/5 nm.

For the analysis of RA, in the first, a series of different volumes (3.0, 6.0, 9.0, 12.0, 15.0, 20.0, 25.0, 30.0, 40.0, 50.0, 60.0, 75.0, 90.0, 105.0 and 120.0 μL) of RA solution (0.03 mM) were added to 75 μL of DCCNa solutions in 10 mL plastic centrifuge tubes. After 2-minute reaction, the 50 μL of PVP-CuNCs solution was added and fixed in 3 mL with BR buffer solution (pH = 4). The remaining steps are consistent with the previous steps. Finally, the selectivity and interference experiments of DCCNa/RA were discussed. All experiments were implemented three times.

Pretreatment and Detection of Actual Samples

All samples were purchased from the local supermarket (Nanchong, China) and they were preprocessed according to previous literatures [32, 33]. For the detection of actual DCCNa samples, a certain amount of pre-treated solution and DCCNa standard solution (0, 0.06, 0.12 and 0.18 μM) and 50 μL of CuNCs were extracted for analysis and detection according to the detection method described in the above section. For the detection of actual RA samples, a certain amount of pretreated solution and 75 μL of DCCNa solution (0.06 mM), 50 μL of CuNCs and RA standard solution (0, 0.06, 0.09 and 0.12 μM) were extracted for analysis and detection accordance according to the detection method described in the above section.

Results and Discussion

Optimization of Synthesis Conditions

In order to obtain good photoluminescence of PVP-CuNCs, its synthesis conditions were optimized. First, the influence of pH was discussed. As shown in Fig. S1A, the fluorescence intensities of PVP-CuNCs at 424 nm increased with the increase of pH (2.5–3.5), and then decreased with the increase of pH (3.5–4.5). It may be attributed to the fact that AA has a stronger reducing capacity in a larger pH environment, reducing Cu^{2+} to large-size non-luminous nanoparticles, while in a lower pH environment, the reducing capacity is not strong [34]. Secondly, the dosage of PVP was optimized, and the fluorescence intensity of PVP-CuNCs at 424 nm was strongest when the concentration of PVP was set at 0.3448 mM (Fig. S1B). Finally, the impact of PVP with different average molecular weights was also discussed under the aforementioned optimal conditions. As shown in Fig. 2A, its fluorescence intensity at 424 nm was the highest when the average molecular weight of PVP was 58000, which might be the higher relative molecular weight of PVP, the larger corresponding hydrated particle size of CuNCs (Fig. 2B–F), resulting in larger particle sizes in DLS measurement and lower fluorescence intensity of PVP-CuNCs at 424 nm. However, the synthesized CuNCs with lower relative molecular weight of PVP also exhibited relatively low fluorescence intensity, possibly because smaller molecular weight might reduce the interaction between PVP and Cu, thus inhibiting the charge transfer of ligands to metals. Also, the solubility of PVP with higher molecular weight in water decreased, causing that the ligands couldn't be effectively attached to metal surfaces [35, 36]. In conclusion, the optimal pH, type and dosage of PVP for the synthesis of PVP-CuNCs were set at 3.5, Mr = 58000 and 0.3448 mM, respectively.

Characterization of PVP-CuNCs

To characterize the PVP-CuNCs, TEM, XPS, FT-IR, UV-vis absorption, and fluorescence spectra were recorded. First of all, the TEM and XPS were measured. As shown in Fig. 3A, PVP-CuNCs were spherical and had good dispersibility in water. And its average diameters were estimated to be 2.21 ± 0.06 nm by the randomly selected 100 nanoparticles (Insert of Fig. 3A). At the same time, the lattice fringe space was measured 0.206 nm (Fig. 3B), which indicated the Cu (111) plane of the nanoclusters [37]. The elemental compositions and states of CuNCs were performed by XPS. The XPS survey spectrum of CuNCs

(Fig. 3C) clearly showed that the copper nanoclusters were composed of C, N, O, and Cu. The high-resolution survey scan of Cu 2p was shown in Fig. 3D, which exhibited two distinct fitting peaks at 932.85 and 952.6 eV, representing $2p^{3/2}$ and $2p^{1/2}$ of Cu, respectively [38]. It indicated that CuNCs were composed of Cu (0) and Cu (I). In addition, since the characteristic peak of 942 eV didn't exist, it further indicated that copper nanoclusters didn't contain Cu (II) [39]. In the high-resolution survey scan of C 1s (Fig. S2A), 284.79, 285.71 and 287.37 eV were the locations of the feature fitting peaks of C-C, C-N and C=O bondings, respectively [40]. In the high-resolution survey scan of N 1s (Fig. S2B), 399.49 eV was the location of the feature-fitting peak of the C-N bonding [41]. In the high-resolution survey scan of O 1s (Fig. S2C), 530.88 and

Fig. 3 TEM images of CuNCs (**A**) (Insert: corresponding the size distribution) and corresponding HRTEM (**B**); XPS survey spectrum of CuNCs (**C**) and high-resolution survey scan of Cu 2p (**D**); Mapping image of CuNCs (**E**); Excitation and emission spectra of CuNCs (**F**, Insert: photographs of CuNCs in sunlight (left cuvette) and 365 nm UV lamp (right cuvette)) ▶

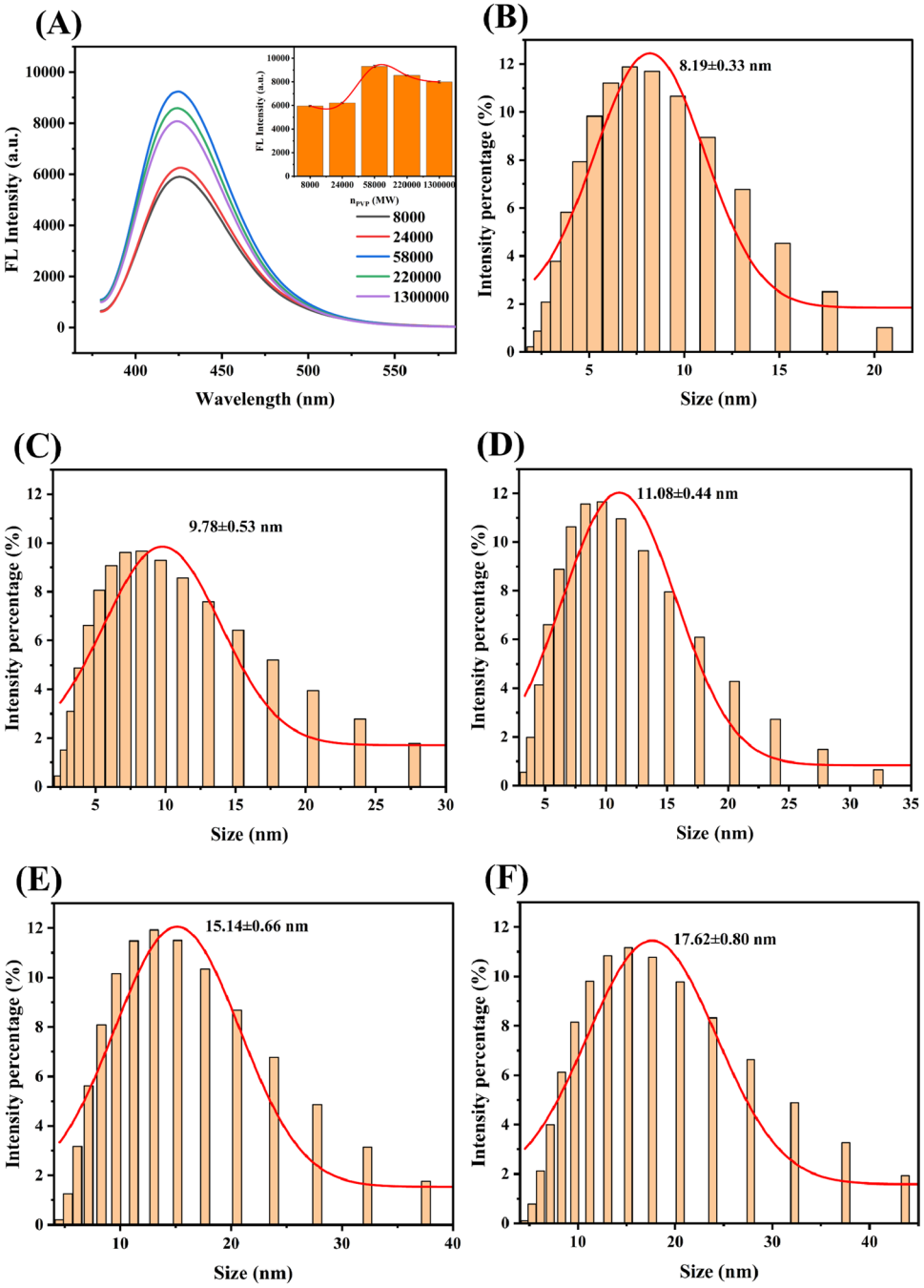

Fig. 2 The influence of PVP with different average molecular weights (**A**) for synthesis; Particle size statistical distribution using dynamic light scattering (DLS) for the PVP-CuNCs (Mr_{pvp} = 8000 (**B**), 24000 (**C**), 58000 (**D**), 220000 (**E**) and 1300000 (**F**)) systems

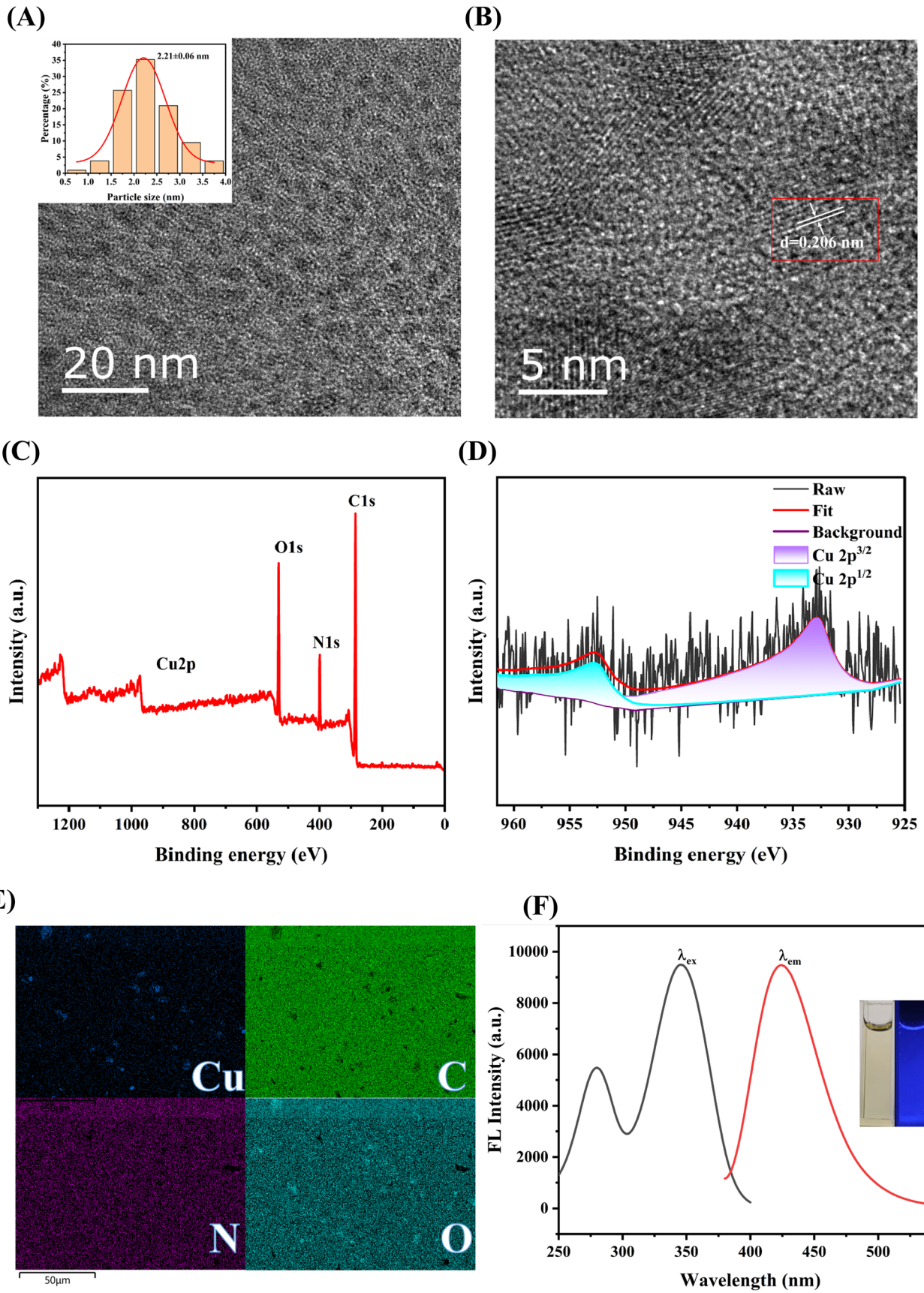
(A)
2.21±0.06 nm
Percentage (%)
Particle size (nm)
20 nm
(B)
d=0.206 nm
5 nm
(C)
C1s
O1s
N1s
Cu2p
Intensity (a.u.)
Binding energy (eV)
(D)
Raw
Fit
Background
Cu 2p3/2
Cu 2p1/2
Intensity (a.u.)
Binding energy (eV)
(E)
Cu
C
N
O
50μm
(F)
λex
λem
FL Intensity (a.u.)
Wavelength (nm)

523.08 eV were the locations of the feature fitting peaks of the C=O bonding and O-H bonding, respectively [42]. Furthermore, elemental analysis of CuNCs was performed (Fig. 3E), it could be clearly seen that elements such as Cu, C, N and O were evenly distributed in the material and corresponding EDX composition was given in the inset of Fig. S3. Additionally, as shown in Fig. S4, the FT-IR spectra showed that the absorption peaks of stretching vibration of -CH bonding was 2952.5 cm^{-1} and deformation vibration of -CH bonding were 1425.2 cm^{-1} and 1373.1 cm^{-1}, and the absorption peaks of C-N and C=O bonding were 1286.3 cm^{-1} and 1672.0 cm^{-1}, respectively, which were consistent with literature reports [43]. That also showed that PVP and PVP-CuNCs had similar absorption peaks, and PVP was successfully attached to the surface of CuNCs. Meanwhile, the UV-vis absorption spectra of PVP and PVP-CuNCs, showed that only the new absorption peak appeared at about 287 nm in the PVP-CuNCs, while there was no surface plasma resonance peak at 500-600 nm (Fig. S5), which indicated that there weren't copper nanoparticles [44]. Then the fluorescence spectra showed the maximum excitation and emission wavelengths of the PVP-CuNCs were 345 nm and 424 nm, respectively (Fig. 3F). And the PVP-CuNCs solution was faint yellow

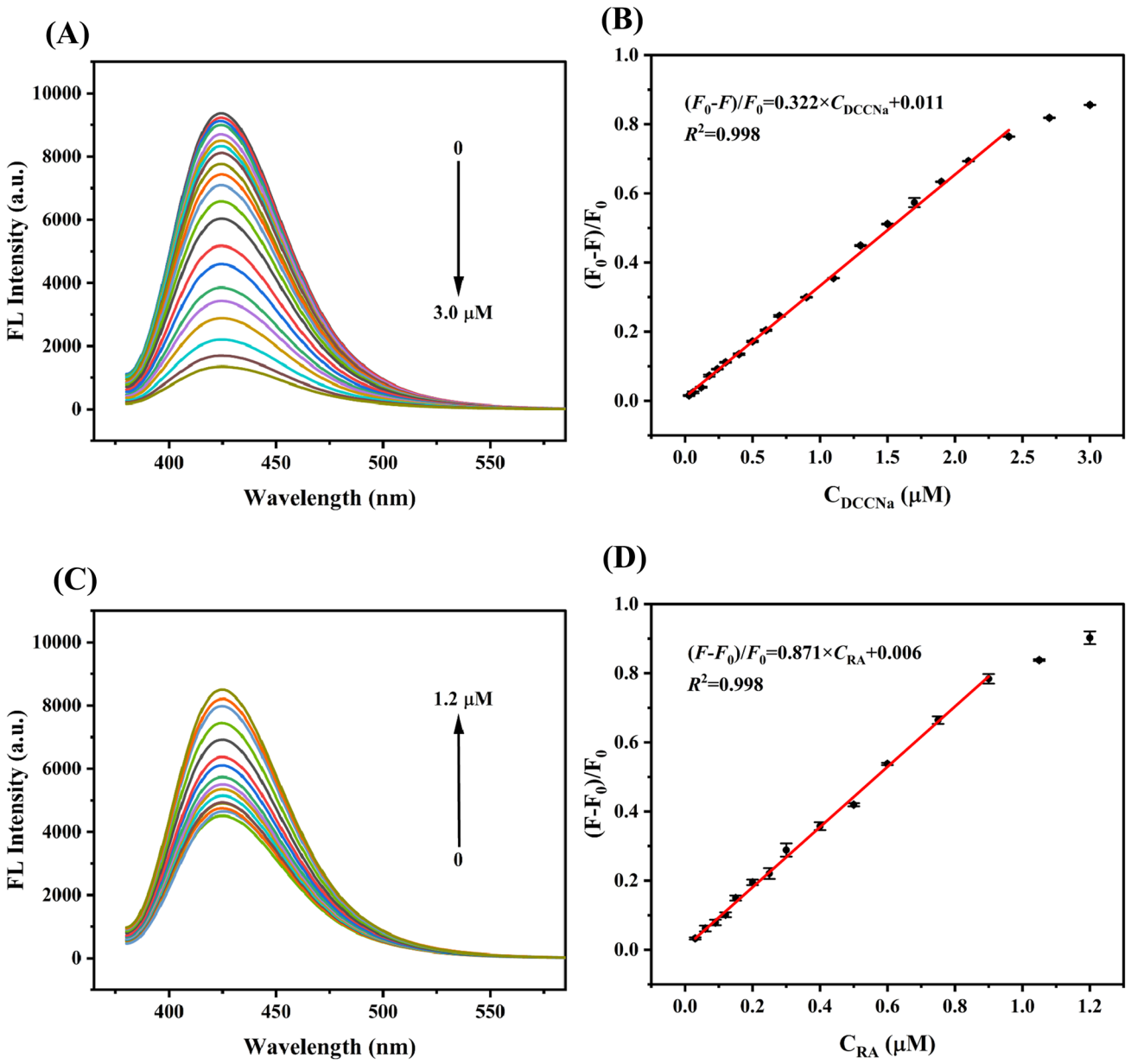

Fig. 4 Fluorescence spectra of PVP-CuNCs after the addition of DCCNa (**A**) and RA (**C**); Linear relationship between the values of $(F_0\text{-}F)/F_0$ and C_{DCCNa} (**B**) and $(F\text{-}F_0)/F_0$ and C_{RA} (**D**)

in sunlight (left cuvette of the insert of Fig. 3F) and blue in a 365 nm UV lamp (right cuvette of the insert of Fig. 3F). In summary, copper nanoclusters were successfully synthesized. Finally, the quantum yield of the PVP-CuNCs was calculated to be 14.97% using quinine sulfate as the reference standard ($\Phi_s = 54\%$).

Stability of PVP-CuNCs

The stability of CuNCs was studied by measuring its fluorescence intensity at 424 nm under different conditions. As shown in Fig. S6A, within the 4–10 range of pH, the fluorescence intensities of CuNCs varied slightly, showing good stability. From Fig. S6B, it could be seen that CuNCs still had a stable fluorescence intensity after 9 days of storage, indicating that it exhibited good storage stability. In addition, the salt resistance of CuNCs as shown in Fig. S6C, in the salt concentration range of 0-200 mM, the fluorescence intensities of CuNCs changed little, indicating its salt stability was better.

Detection of DCCNa

In order to obtain the best detection conditions, the effects of pH, reaction time and temperature were discussed. The optimal reaction conditions were obtained as follows: pH value of BR buffer, reaction time, and reaction temperature

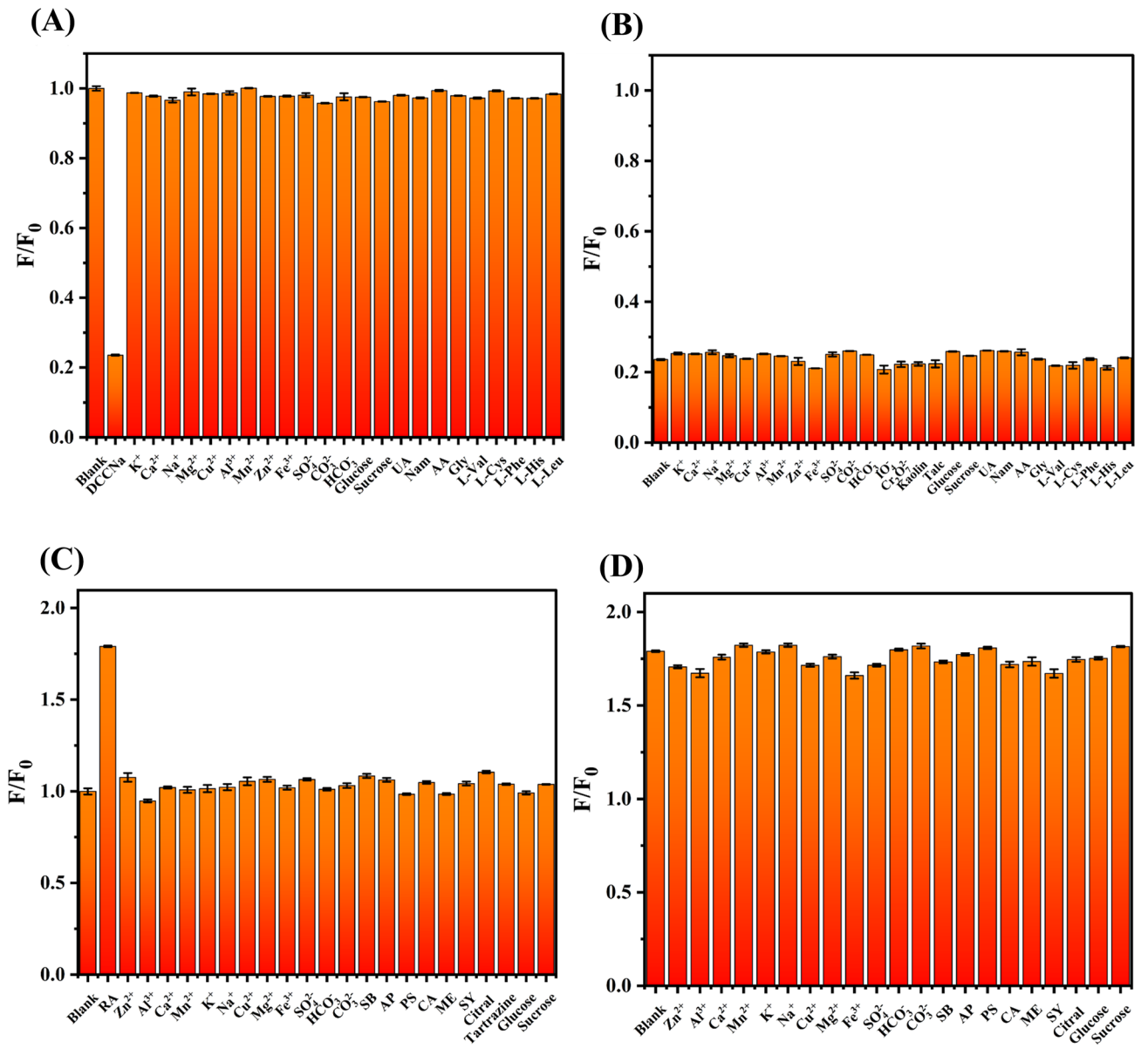

Fig. 5 The selectivity of PVP-CuNCs (**A**) and PVP-CuNCs-DCCNa (**C**) to different materials; The fluorescence intensity ratios of PVP-CuNCs-DCCNa (**B**) and PVP-CuNCs-DCCNa-RA (**D**) systems in the different coexistent materials

were 3.5, 1.0 min, and 25℃, respectively (Fig. S7A–C). Thus, DCCNa was detected under the optimal conditions. As shown in Fig. 4A, when different concentrations of DCCNa were added to the PVP-CuNCs system, the fluorescence intensity (424 nm) of PVP-CuNCs gradually decreased with the increase of DCCNa concentration. In the range of 0.030-2.400 μM, the linear fitting curve was obtained according to the relationship between $(F_0\text{-}F)/F_0$ and DCCNa concentration (Fig. 4B). The linear fitting equation was $(F_0\text{-}F)/F_0 = 0.322 \times C_{DCCNa} + 0.011$ ($R^2 = 0.998$, F_0 and F represent the FL intensities of PVP-CuNCs without and with the addition of DCCNa), and the corresponding limit of detection (LOD) was calculated to be 10.766 nM (3σ/K).

Detection of RA

To obtain the best detection conditions, the reaction time of DCCNa and RA was discussed. As shown in Fig. S7D, the fluorescence intensity did not change significantly after 2 min of reaction. As shown in Fig. 4C, when different concentrations of RA were added to the PVP-CuNCs-DCCNa detection system, the fluorescence intensity gradually at 424 nm increased with the increase of RA concentration. In the range of 0.030-0.900 μM, a linear fitting curve was obtained according to the relationship between $(F\text{-}F_0)/F_0$ value and RA concentration (Fig. 4D). The linear fitting equation was $(F\text{-}F_0)/F_0 = 0.871 \times C_{RA} + 0.006$ ($R^2 = 0.998$,

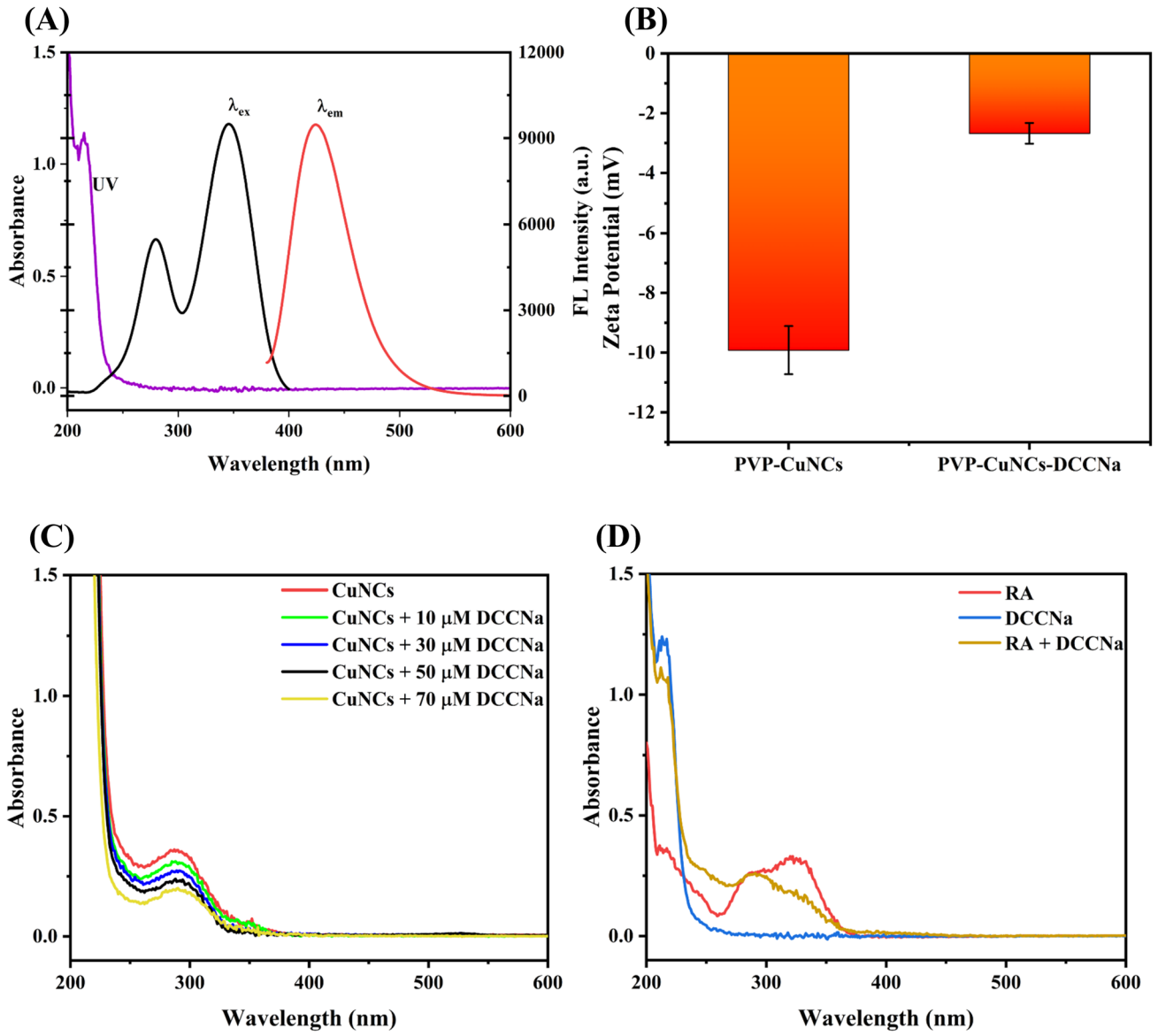

Fig. 6 The UV-vis absorption spectrum of DCCNa and the fluorescence excitation and emission spectra of CuNCs (**A**); The zeta potential of PVP-CuNCs without and with the addition of DCCNa (**B**); The UV-vis absorption spectra before and after adding DCCNa of CuNCs (**C**); The UV-vis absorption spectra of RA, DCCNa and RA + DCCNa (**D**)

F_0 and F represent the FL intensities of PVP-CuNCs without and with the addition of RA), and corresponding LOD was calculated to be 8.985 nM (3σ/K). In addition, we compared the LOD and detection range of other methods. As shown in Table S1, the built method had a lower LOD.

Selectivity and Interference Testing of DCCNa

To verify the selectivity of CuNCs for DCCNa, several representative substances were studied, such as K^+, Ca^{2+}, Na^+, Mg^{2+}, Cu^{2+}, Al^{3+}, Mn^{2+}, Zn^{2+}, Fe^{3+}, SO_4^{2-}, CO_3^{2-}, HCO^{3-}, IO_4^-, $Cr_2O_7^{2-}$, glucose, sucrose, UA, Nam, AA, Gly, L-Val, L-Cys, L-Phe, L-His and L-Leu. It could be seen from Fig. 5A that only DCCNa caused the fluorescence of CuNCs to decrease significantly, indicating that it had good selectivity. Some substances such as kaolin, talc, and some of the above-mentioned substances may be present in the real sample as potential interfering substances. When DCCNa and interfering substances were present at the same time, anti-interference tests were conducted. As could be seen from Fig. 5B, the changes of fluorescence intensities at 424 nm were not obvious, indicating that it had good anti-interference ability.

Selectivity and Interference Testing of RA

To verify the selectivity of the PVP-CuNCs-DCCNA system for RA, some representative substances were studied, such as K^+, Ca^{2+}, Na^+, Mg^{2+}, Cu^{2+}, Al^{3+}, Mn^{2+}, Zn^{2+}, Fe^{3+}, SO_4^{2-}, CO_3^{2-}, HCO^{3-}, glucose, sucrose, SB, AP, PS, CA, ME, SY, citral and tartrazine. As could be seen from Fig. 5C, only RA caused the fluorescence of the system to increase significantly, indicating that it had good selectivity. Some of the above-mentioned substances may be present in the real sample as potential interfering substances. In the case of RA and interfering substances being present at the same time, anti-interference tests were conducted. As could be seen from Fig. 5D, the changes of fluorescence intensities at 424 nm were not obvious, indicating that it had good anti-interference ability.

The Fluorescence Quenching Mechanism of PVP-CuNCs by DCCNa

As described in Fig. 6A, little overlap between the UV-vis absorption spectrum of DCCNa and fluorescence excitation/emission spectrum of PVP-CuNCs was observed, hinting that the quenching mechanism of CuNCs by DCCNa was neither due to the inner filter effect (IFE) nor Förster resonance energy transfer (FRET) [45, 46]. Additionally, the Zeta potential of CuNCs increased to -2.68 mV after the addition of DCCNa, indicating the oxidation of copper on the surface of the CuNCs to Cu^{2+}, resulting in a decrease in negative charge (Fig. 6B). The oxidation reaction of CuNCs in the presence of DCCNa may be related to Eqs. (1) and (2). At the same time, after the addition of DCCNa, no new absorption peak appeared in the UV-vis absorption spectrum of CuNCs, and the UV-vis absorption peak at 287 nm gradually decreased with increasing concentrations of DCCNa (Fig. 6C), which reconfirmed that the copper on the surface of the CuNCs was oxidized. In conclusion, the quenching mechanism of PVP-CuNCs by DCCNa was oxidative quenching, i.e., copper on the surface of CuNCs was oxidized to Cu^{2+}.

Table 1 The assays of DCCNa and RA by the CuNCs-PVP and CuNCs-PVP-DCCNa probe, respectively ($n = 3$)

DCCNa					RA				
Samples	Added (μM)	Found* (μM)	Recovery (%)	RSD (%)	Samples	Added (μM)	Found* (μM)	Recovery (%)	RSD (%)
	0	0.251 ± 0.001	-	0.54		0	0.443 ± 0.006	-	1.33
Swimming pool water	0.06	0.313 ± 0.003	103.0	0.80	RA additive	0.06	0.502 ± 0.004	98.8	0.70
	0.12	0.377 ± 0.003	104.8	0.82		0.09	0.534 ± 0.004	100.9	0.73
	0.18	0.436 ± 0.006	102.5	1.49		0.12	0.559 ± 0.002	96.6	0.36
	0	0.366 ± 0.004	-	1.17		0	0.392 ± 0.007	-	1.67
DCCNa pesticide powder	0.06	0.429 ± 0.005	104.1	1.26	Thyme extract	0.06	0.450 ± 0.005	97.2	1.12
	0.12	0.481 ± 0.007	95.8	1.38		0.09	0.487 ± 0.003	105.4	0.62
	0.18	0.546 ± 0.010	99.8	1.89		0.12	0.517 ± 0.006	104.7	1.20
	0	-	-	-		0	0.344 ± 0.005	-	1.46
Soil extract	0.06	0.063 ± 0.001	104.9	1.08	Basil extract	0.06	0.406 ± 0.010	102.6	2.54
	0.12	0.120 ± 0.002	100.2	1.58		0.09	0.434 ± 0.007	100.2	1.69
	0.18	0.178 ± 0.003	98.8	1.78		0.12	0.471 ± 0.006	105.6	1.37

*The confidence range was set at 95%

Table 2 Comparison of the detection result of DCCNa and RA by the work and standard methods ($n = 3$)

DCCNa*			RA*		
Samples	This work	Titration	Samples	This work	HPLC
Swimming pool water	1.659 ± 0.009 mg/kg	1.650 ± 0.011 mg/kg	RA additive	88.606 ± 1.182 mg/g	87.889 ± 2.357 mg/g
DCCNa pesticide powder	244.056 ± 2.850 mg/g	240.010 ± 4.013 mg/g	Thyme extract	1.694 ± 0.028 mg/g	1.709 ± 0.052 mg/g
Soil extract	Not detected	Not detected	Basil extract	1.487 ± 0.022 mg/g	1.462 ± 0.014 mg/g

*The confidence range was set at 95%

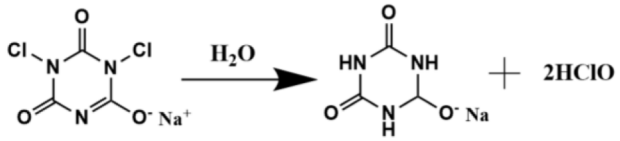

(1)

$$Cu + HClO + H^+ \rightarrow Cu^{2+} + Cl^- + H_2O \quad (2)$$

The Mechanism of Fluorescence Increase by RA

From Fig. 6D, there was a shift in the ultraviolet absorption peak of RA when it was mixed with DCCNa. This is because RA possesses antioxidant properties and can react with DCCNa, and the phenomenon can be explained by Eq. (3) [47]. Due to the reaction between RA and DCCNa, which leaded to a decrease in the concentration of HClO, thereby causing an increase in fluorescence intensity.

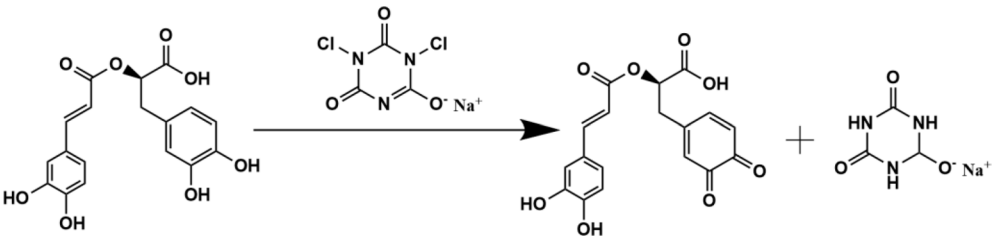

(3)

Analysis of Actual Samples

To verify the reliability of the method, intra-day and inter-day detection results of DCCNa/RA were analyzed (Table S2). The RSD values were less than 2.22%/2.69%, indicating that the method had certain reliability. In order to further verify the application of this method in real samples, three real samples were selected, and corresponding results were analyzed by standard addition experiment. As shown in Table 1, the recoveries of DCCNa/RA were 95.8-104.9%/96.6-105.6%, and the RSD were less than 1.89%/2.54%. In addition, other standard methods (like titration and HPLC) were used to detect the actual samples (Table 2), and the results between the two were not significantly different. In summary, the method had a certain detection ability.

Conclusions

In this work, blue-emitting CuNCs were synthesized for the detection of DCCNa/RA by one-step method. For the DCCNa/RA assay, corresponding linear ranges were 0.030–2.400/0.030-0.900 μM as well as LOD were 10.766/8.985 nM. The method could be used for the assay of DCCNa/RA in real samples with high recovery. At the same time, the reaction mechanisms of PVP-CuNCs-DCCNa and PVP-CuNCs-DCCNa-RA systems were also discussed. That is, hypochlorous acid produced by DCCNa dissolved in water has strong oxidation, which will oxidize Cu on the surface of CuNCs to Cu^{2+}, causing the fluorescence quenching of PVP-CuNCs. While RA has antioxidant properties and can react with hypochlorous acid to restore fluorescence by reducing the generation of hypochlorous acid.

Supplementary Information The online version contains supplementary material available at https://doi.org/10.1007/s10895-023-03454-2.

Author Contributions Conceptualization, methodology, investigation and writing: [Jianhua Kuang]; Methodology and investigation: [Qingqing Hu]; Analysis: [Yao Feng]; Reviewing: [Jingxue Yuan]; Conceptualization, methodology, original draft and revision: [Zhengjun Cheng].

Funding The authors gratefully acknowledge financial support from the Natural Science Foundation of Sichuan Province (2023NSFSC0354), and Doctor Start-up Fund (15E006) of China West Normal University.

Data Availability All data generated or analyzed during this study are included in this published article and its supplementary information file.

Declarations

Ethics Approval Not applicable.

Consent to Participate Not applicable.

Consent to Publish Not applicable.

Competing Interests The authors have no relevant financial or non-financial interests to disclose.

References

1. Proto A, Zarrella I, Cucciniello R, Pironti C, Caro FD, Motta O (2016) Bactericidal and fungicidal activity in the gas phase of Sodium Dichloroisocyanurate (NaDCC). Curr Microbiol 73(2):287–291. https://doi.org/10.1007/s00284-016-1040-x
2. Dong Y, Gu M, Yuan H, Zhu N (2021) Insights into the enhancement of waste activated sludge dewaterability using sodium dichloroisocyanurate and dodecyl dimethyl ammonium chloride: performance, mechanism, and implication. Sci Total Environ 778. https://doi.org/10.1016/j.scitotenv.2021.146302
3. Morgenthau A, Nicolae AM, Laursen AE, Foucher DA, Wolfaardt GM, Hausner M (2012) Assessment of the working range and effect of sodium dichloroisocyanurate on Pseudomonas aeruginosa biofilms and planktonic cells. Biofouling 28(1):111–120. https://doi.org/10.1080/08927014.2011.654335
4. Park CM, Jeon S, Kim YH, Kim J, Choi SJ, Shim I, Eom IC, Han SC, Kim MS (2022) Sodium dichloroisocyanurate toxicity in rats during a 90-day inhalation toxicity study. Toxicol Appl Pharm 456. https://doi.org/10.1016/j.taap.2022.116279
5. Sun W, Zhao X, Wan Y, Yang Y, Li X, Chen X, Mei Y, An L (2023) Prenatal cyanuric acid exposure induced spatial learning impairments associated with alteration of acetylcholine-mediated neural information flow at the hippocampal CA3-CA1 synapses of male rats. Hum Exp Toxicol 42. https://doi.org/10.1177/09603271231163477
6. Sathyanarayana S, Flynn JT, Messito MJ, Gross R, Whitlock KB, Kannan K, Karthikraj R, Morrison D, Huie M, Christakis D, Trasande L (2019) Melamine and cyanuric acid exposure and kidney injury in US children. Environ Res 171:18–23. https://doi.org/10.1016/j.envres.2018.10.038
7. Petersen M (2013) Rosmarinic acid: new aspects. Phytochem Rev 12(1):207–227. https://doi.org/10.1007/s11101-013-9282-8
8. Marchev AS, Vasileva LV, Amirova KM, Savova MS, Koycheva IK, Balcheva-Sivenova ZP, Vasileva SM, Georgiev MI (2021) Rosmarinic acid - from bench to valuable applications in food industry. Trends Food Sci Tech 117:182–193. https://doi.org/10.1016/j.tifs.2021.03.015
9. Dahchour A (2022) Anxiolytic and antidepressive potentials of rosmarinic acid: a review with a focus on antioxidant and anti-inflammatory effects. Pharmacol Res 184. https://doi.org/10.1016/j.phrs.2022.106421
10. Zhang W, Cheng C, Sha Z, Chen C, Yu C, Lv N, Ji P, Wu X, Ma T, Cheng H, Shi L (2021) Rosmarinic acid prevents refractory bacterial pneumonia through regulating Keap1/Nrf2-mediated autophagic pathway and mitochondrial oxidative stress. Free Radical Bio Med 168:247–257. https://doi.org/10.1016/j.freeradbiomed.2021.03.038
11. Veras KS, Fachel FNS, Teixeira HF, Koester LS (2022) Technological strategies applied for rosmarinic acid delivery through different routes – A review. J Drug Deliv Sci Tec 68. https://doi.org/10.1016/j.jddst.2021.103054
12. Casanova F, Estevinho BN, Santos L (2016) Preliminary studies of rosmarinic acid microencapsulation with chitosan and modified chitosan for topical delivery. Powder Technol 297:44–49. https://doi.org/10.1016/j.powtec.2016.04.014
13. Patel K, Jones K (2007) Analytical method for the quantitative determination of cyanuric acid as the degradation product of sodium dichloroisocyanurate in urine by liquid chromatography mass spectrometry. J Chromatogr B 853(1):360–363. https://doi.org/10.1016/j.jchromb.2007.03.014
14. Tzing SH, Ding WH (2010) Determination of melamine and cyanuric acid in powdered milk using injection-port derivatization and gas chromatography–tandem mass spectrometry with furan chemical ionization. J Chromatogr A 1217(40):6267–6273. https://doi.org/10.1016/j.chroma.2010.07.081
15. Soto NO, Horstkotte B, March JG, Alba PLd, Martínez LL, Martín VC (2008) An environmental friendly method for the automatic determination of hypochlorite in commercial products using multisyringe flow injection analysis. Anal Chim Acta 611(2):182–186. https://doi.org/10.1016/j.aca.2008.01.073
16. Song X, Shen H, Yin X, Wang X, Liu J (2013) Microflow-injection chemiluminescence of luminol and hypochlorite enhanced by phloxine B. Luminescence 28(1):16–22. https://doi.org/10.1002/bio.1388
17. Talebi S, Rahmati B, Jorjani M, Emadi F, Ghaffari F, Naseri M (2022) Synergistic effects of Nepeta menthoides and Melissa officinalis aqueous extracts on reserpine-induced depressive-like behaviors in mice. Phytother Res 36(6):2481–2494. https://doi.org/10.1002/ptr.7457
18. Shanaida M, Jasicka-Misiak I, Makowicz E, Stanek N, Shanaida V, Wieczorek PP (2020) Development of high-performance thin layer chromatography method for identification of phenolic compounds and quantification of rosmarinic acid content in some species of the Lamiaceae family. J Pharm Bioallied Sc 12(2):139–145. https://doi.org/10.4103/jpbs.JPBS_322_19
19. Özdokur KV, Koçak ÇC (2019) Simultaneous determination of Rosmarinic Acid and Protocatechuic Acid at Poly(o-Phenylenediamine)/Pt nanoparticles modified glassy Carbon Electrode. Electroanal 31(12):2359–2367. https://doi.org/10.1002/elan.201900144
20. Zou T, Li S, Yao G, Qu R, Yang W, Wang H, Tan W, Yang M (2023) Highly photoluminescent tryptophan-coated copper nanoclusters based turn-off fluorescent probe for determination of tetracyclines. Chemosphere 338. https://doi.org/10.1016/j.chemosphere.2023.139452
21. Yin B, Zhang S, Chen H, Yan L (2021) A cationic organic dye based on coumarin fluorophore for the detection of N_2H_4 in water and gas. Sens Actuat B Chem 344
22. Abd Elhaleem SM, Elsebaei F, Shalan S, Belal F (2022) Turn-off fluorescence of nitrogen and sulfur carbon quantum dots as effective fluorescent probes for determination of imatinib. Application to biological fluids. Spectrochim Acta A 272. https://doi.org/10.1016/j.saa.2022.120954
23. Abd Elhaleem SM, Shalan S, Belal F, Elsebaei F (2022) Insights for applying N,S-doped carbon dots as a fluorescent nanoprobe for estimation of some nitro-calcium channel blockers. Roy Soc Open Sci 9(10). https://doi.org/10.1098/rsos.220609
24. Abd Elhaleem SM, Elsebaei F, Shalan S, Belal F (2022) Utilization of N,S-doped carbon dots as a fluorescent nanosensor for determination of cromolyn based on inner filter effect: application to aqueous humour. Luminescence 37(5):713–721. https://doi.org/10.1002/bio.4212
25. Zhang L, Wang E (2014) Metal nanoclusters: New fluorescent probes for sensors and bioimaging. Nano Today 9(1):132–157. https://doi.org/10.1016/j.nantod.2014.02.010

26. Maruthupandi M, Thiruppathi D, Vasimalai N (2020) One minute synthesis of green fluorescent copper nanocluster: the preparation of smartphone aided paper-based kit for on-site monitoring of nanomolar level mercury and sulfide ions in environmental samples. J Hazard Mater 392. https://doi.org/10.1016/j.jhazmat.2020.122294
27. Bhamore JR, Jha S, Mungara AK, Singhal RK, Sonkeshariya D, Kailasa SK (2016) One-step green synthetic approach for the preparation of multicolor emitting copper nanoclusters and their applications in chemical species sensing and bioimaging. Biosens Bioelectron 80:243–248. https://doi.org/10.1016/j.bios.2016.01.066
28. Vilar-Vidal N, Rivas J, López-Quintela MA (2012) Size dependent catalytic activity of Reusable Subnanometer copper(0) clusters. ACS Catal 2(8):1693–1697. https://doi.org/10.1021/cs300355n
29. Kang J, Gao P, Zhang G, Shi L, Zhou Y, Wu J, Shuang S, Zhang Y (2022) Rapid sonochemical synthesis of copper nanoclusters with red fluorescence for highly sensitive detection of silver ions. Microchem J 178. https://doi.org/10.1016/j.microc.2022.107370
30. Yu W, Hu Q, Kuang J, Liao Y, Cheng Z (2023) A ratiometric fluorescent based on orange light emitting copper nanoclusters for sensitive detection of O-phenylenediamine and rosmarinic acid. Chin J Anal Chem 51(7). https://doi.org/10.1016/j.cjac.2023.100284
31. Pena-Pereira F, Capón N, Calle IDI, Lavilla I, Bendicho C (2019) Fluorescent poly(vinylpyrrolidone)-supported copper nanoclusters in miniaturized analytical systems for iodine sensing. Sens Actuat B Chem 299
32. Mo M, Wang X, Ye L, Su Y, Zhong Y, Zhao L, Zhou Y, Peng J (2022) A simple paper-based ratiometric luminescent sensor for tetracyclines using copper nanocluster-europium hybrid nanoprobes. Anal Chim Acta 1190. https://doi.org/10.1016/j.aca.2021.339257
33. Ngo YL, Lau CH, Chua LS (2018) Review on rosmarinic acid extraction, fractionation and its anti-diabetic potential. Food Chem Toxicol 121:687–700. https://doi.org/10.1016/j.fct.2018.09.064
34. Lin YT, Liang C (2013) Carbon Tetrachloride Degradation by Alkaline ascorbic acid solution. Environ Sci Technol 47(7):3299–3307. https://doi.org/10.1021/es304441e
35. Wu H, Wang G, Cai Z, Li D, Xiao F, Lei D, Dai Z, Dou X (2022) Polyethyleneimine-capped copper nanoclusters for detection and discrimination of 2,4,6-trinitrotoluene and 2,4,6-trinitrophenol. Anal Methods UK 14(44):4485–4494. https://doi.org/10.1039/D2AY01311H
36. Wu FN, Zhu J, Weng GJ, Li JJ, Chen XW, Zhao JW (2023) Electron transfer-based norepinephrine detection with high sensitivity regulated by polyethyleneimine molecular weight. Sens Actuat B Chem 379
37. Zheng X, Chen Q, Zhang Z, Wang Z, Gong Z (2022) An aggregation-induced emission copper nanoclusters fluorescence probe for the sensitive detection of tetracycline. Microchem J 180. https://doi.org/10.1016/j.microc.2022.107570
38. Pandit S, Kundu S (2020) pH-Dependent reversible emission behaviour of lysozyme coated fluorescent copper nanoclusters. J Lumin 228. https://doi.org/10.1016/j.jlumin.2020.117607
39. Shen J, Fan Z (2023) Ce^{3+}-induced fluorescence amplification of copper nanoclusters based on aggregation-induced Emission for specific sensing 2,6-pyridine Dicarboxylic Acid. J Fluoresc 33(1):135–144. https://doi.org/10.1007/s10895-022-03044-8
40. Han Y, Chen Y, Feng J, Liu J, Ma S, Chen X (2017) One-Pot synthesis of fluorescent Silicon Nanoparticles for sensitive and selective determination of 2,4,6-Trinitrophenol in aqueous solution. Anal Chem 89(5):3001–3008. https://doi.org/10.1021/acs.analchem.6b04509
41. Huang J, Zhang M, Huang J, Deng X, Zhang X, Miao C, Weng S (2023) Detection of doxycycline using Carbon Quantum dots as probe based on Internal Filtering Effect. J Fluoresc 34(8):108099. https://doi.org/10.1007/s10895-023-03373-2
42. Jia J, Lin B, Gao Y, Jiao Y, Li L, Dong C, Shuang S (2019) Highly luminescent N-doped carbon dots from black soya beans for free radical scavenging, Fe^{3+} sensing and cellular imaging. Spectrochim Acta A 211:363–372. https://doi.org/10.1016/j.saa.2018.12.034
43. Cai Z, Zhang Y, Zhang Y, Bai Y, Huang J, Guo Z, Bao H, Zhang J (2023) One-pot simple preparation of bright blue emitting copper nanoclusters for sensitive detection of chrysin via inner filter effect. J Lumin 257. https://doi.org/10.1016/j.jlumin.2023.119781
44. Khataee A, Jalili R, Dastborhan M, Karimi A, Azar AEF (2020) Ratiometric visual detection of tetracycline residues in milk by framework-enhanced fluorescence of gold and copper nanoclusters. Spectrochim Acta A 242. https://doi.org/10.1016/j.saa.2020.118715
45. Cai Z, Pang S, Wu L, Hao E, Rong J (2021) Highly sensitive and selective fluorescence sensing of nitrofurantoin based on water-soluble copper nanoclusters. Spectrochim Acta A 255. https://doi.org/10.1016/j.saa.2021.119737
46. Wang M, Zhang J, Zhou X, Sun H, Su X (2022) Fluorescence sensing strategy for xanthine assay based on gold nanoclusters and nanozyme. Sens Actuat B Chem 358
47. Fujimoto A, Masuda T (2012) Antioxidation mechanism of rosmarinic acid, identification of an unstable quinone derivative by the addition of odourless thiol. Food Chem 132(2):901–906. https://doi.org/10.1016/j.foodchem.2011.11.062